Frictional Effects in Strongly Divergent Flows

JULIA PAEGLE[1,2] AND JAN PAEGLE

National Center for Atmospheric Research,[3] Boulder, CO 80307

(Manuscript received 1 November 1977, in final form 15 March 1978)

ABSTRACT

The effect of friction in strongly divergent steady flows is studied. It is found that friction weakens flow divergence out of strong high-pressure centers, contrary to the more commonly studied case for weaker high-pressure centers in rotating flows, for which friction produces divergence. The stability of the solution is discussed for the general case on a linear basis. Nonlinear analytic solutions are presented for the case of no deformation in the flow. The conclusions are quantified in a drag, deformation and Laplacian of geopotential parameter space.

1. Introduction

Although atmosphere divergence is often small in comparison to other measures of wind variability, its existence is crucial to the total flow energetics and to the actual weather. Consequently, correct simulation of divergence in numerical forecast models is essential to accurate numerical prediction. This is one reason for the large number of idealized studies attempting to isolate various dynamical causes of convergence (e.g., Ekman pumping, gravity waves, topography, fronts, land-sea, mountain-valley breezes, omega equation forcings, etc.). Although all of these mechanisms are not entirely distinct, it often proves instructive to isolate their effects in order to conceptualize their influences in particular events, as well as to systematize improvement of forecast models.

This paper continues our investigation of a relatively less studied dynamical basis for atmospheric flow divergence, which was apparently first suggested in a meteorological context by Syono (1948) and later by Miyakoda (1956). In simplest terms, it may be idealized as divergence driven by a high-pressure field strong enough that the total horizontal force field is divergent.

In the case of absolutely divergent ("supergradient") high-pressure fields, a steady, purely rotational flow cannot be established, since its convergent centripetal acceleration cannot balance the divergent force field. This represents the situation for which the gradient wind solution is complex and the balance equation is non-elliptic. These equations fail because their underlying assumption of solenoidal flow is incompatible with the divergent force field.

Although the physical picture is simple, its dynamics has been relatively neglected within data and theoretical studies until recently. One reason for this may be that no clear-cut observational studies of the phenomena were available. Another reason may be that the circumstances of nonreal gradient wind are also ones for which instability (with respect to gradient flow) may arise, thereby inhibiting any pronounced development of a supergradient force field.

However, stable flow evolution may actually exist in these "supergradient" cases if the balanced basic state flow is recognized to be divergent rather than solenoidal. This is discussed by Paegle and Paegle (1976b, hereafter referred to as I). The relevance of such divergent flow solutions to synoptic-scale events is suggested in data investigations by MacDonald (1977) and Paegle and Paegle (1976a) who find frequent occurrences of supergradient pressure fields in the upper troposphere. The former study shows association with heavy convection and severe weather and the latter suggests a link to global-scale flows. The divergence diagnosed from many of these cases is qualitatively similar to observed divergences, although magnitudes are often different.

The main purpose of the present study is to include the influence of frictional drag in the analyses we performed in I. The need for this is indicated by the common association of the supergradient regions with strong convection (MacDonald, 1977), the implied frictional effect of convection through vorticity mixing (Reed and Johnson, 1974; Holton and Colton, 1972; Lindzen, 1974; and others), and the general divergence overestimation that our previous frictionless diagnostic estimates produce.

The effect of friction is included through a simple

[1] The authors were on leave from the Department of Meteorology, University of Utah.

[2] Work completed while at the Department of Atmospheric Sciences, UCLA.

[3] The National Center for Atmospheric Research is sponsored by the National Science Foundation.

0022-4928/78/1197-1203$05.00

drag formulation. This is done because the observational estimates (Norquist *et al.*, 1977; Holton and Colton, 1972) of dissipation times are most directly translated into drag coefficients and this simple formulation is perhaps to the level of other simplifications (elaborated in I).

The basic conclusion is that friction weakens flow divergence out of supergradient pressure patterns contrary to the more commonly studied case for weaker high-pressure centers in rotating flows for which friction produces divergence. Less obvious conclusions relate to the destabilizing influence of deformation in the geostrophic pattern and the damping of flow divergence with very strong friction even in gradient cases. These conclusions are quantified in a drag, deformation and Laplacian of geopotential parameter space.

2. Linearized analysis

The equations are the same as those used in I except for the inclusion of a drag coefficient μ. Part of the following analysis is similar to that of I but is repeated here for the sake of clarity.

The analysis is based on the divergence, vorticity and deformation equations in Cartesian coordinates, neglecting tilting terms associated with horizontal variation of vertical motion:

$$\frac{dD}{dt}=\tfrac{1}{2}[\eta^2-(A^2+B^2+D^2)]-(\nabla^2\phi+\tfrac{1}{2}f^2-\tfrac{1}{2}\mu^2), \quad (1)$$

$$\frac{dA}{dt}=-DA+f(B-B_g), \quad (2)$$

$$\frac{dB}{dt}=-DB-f(A-A_g), \quad (3)$$

$$\frac{d\eta}{dt}=-\eta D+\mu f, \quad (4)$$

where

$$\left.\begin{aligned} D&=u_x+v_y+\mu, & \eta&=v_x-u_y+f\\ A&=v_x+u_y, & A_g&=f^{-1}(\phi_{xx}-\phi_{yy})\\ B&=v_y-u_x, & B_g&=2f^{-1}\phi_{xy}\end{aligned}\right\}$$

and ϕ is the geopotential. We also assume that f, $\nabla^2\phi$, A_g and B_g are constant.

Solutions to (1)–(4) give time changes of the flow kinematics following trajectories (Lagrangian coordinates) or can be considered as local time changes if advective effects are negligible.

Then, a Lagrangian steady-state solution of Eqs. (1)–(4) is given by

$$A=A_s=\frac{A_g-(D_s/f)B_g}{1+D_s^2/f^2}, \quad (5)$$

$$B=B_s=\frac{B_g+(D_s/f)A_g}{1+D_s^2/f^2}, \quad (6)$$

$$\eta=\eta_s=\mu f/D_s, \quad (7)$$

where D_s satisfies the algebraic equation

$$\frac{(\mu f)^2}{D_s^2}-D_s^2-\frac{A_g^2+B_g^2}{1+D_s^2/f^2}-(2\nabla^2\phi+f^2)+\mu^2=0. \quad (8)$$

From Eqs. (5)–(8) and the assumptions previously stated it follows that A_s, B_s, η_s and D_s are also constants.

For the particular case $\mu=0$, Eq. (8) reduces to a quadratic equation in D_s^2. In this case (5)–(8) represent stable steady-state solutions for high-pressure centers which are sufficiently strong that $2\nabla^2\phi+f^2+A_g^2+B_g^2\leqslant 0$. We have discussed the characteristics and realizability of these solutions in I and in other related papers (Paegle and Paegle, 1974, 1976a).

The solution to the inviscid case, which corresponds to the gradient wind solution for the limiting case of $2\nabla^2\phi+f^2=0$ and $A_g^2+B_g^2=0$, is

$$D_s^2=-(f^2+\nabla^2\phi)+|f[(f^{-1}\nabla^2\phi)^2-(A_g^2+B_g^2)]^{\frac{1}{2}}|. \quad (9)$$

For the viscous case (8) is a cubic equation in D_s^2. The root that corresponds to (9) for the limiting case of no viscosity and for $2\nabla^2\phi+f^2+A_g^2+B_g^2<0$ is

$$D_s^2=\begin{cases}[-\frac{1}{2}b+c^{\frac{1}{2}}]^{\frac{1}{3}}+[-\frac{1}{2}b-c^{\frac{1}{2}}]^{\frac{1}{3}}-\frac{1}{3}p, & c>0\\ [\frac{1}{2}b]^{\frac{1}{3}}-\frac{1}{3}p, & \\ \quad c=0,\ \mu=0 \text{ and } 2\nabla^2\phi+f^2+A_g^2+B_g^2=0 & \\ 2[-\frac{1}{3}a]^{\frac{1}{2}}\cos\frac{1}{3}\phi-\frac{1}{3}p, & c<0\end{cases} \quad (10)$$

where

$$p=2(f^2+\nabla^2\phi)-\mu^2,$$

$$a=f^2(A_g^2+B_g^2+2\nabla^2\phi+f^2-2\mu^2)-(p^2/3),$$

$$b=(1/27)[2p^3-9pf^2(A_g^2+B_g^2+2\nabla^2\phi+f^2-2\mu^2)]-\mu^2f^4,$$

$$c=(b^2/4)+(a^3/27),$$

$$\phi=\cos^{-1}[-0.5b/(-a^3/27)^{\frac{1}{2}}].$$

In this viscous case the solutions given by (5), (6), (7) and (10) may be either stable or unstable depending upon the various parameters of the problem. Therefore, a linear stability analysis is performed to delineate the characteristic of the solution for a physically meaningful region of the parameter space.

For this, new variables are defined such that $D'=D-D_s$, $A'=A-A_s$, $B'=B-B_s$ and $\eta'=\eta-\eta_s$ and four equations similar to (1)–(4) are obtained. Expanding the right-hand side of these in a Taylor

series about the origin, the first order result is

$$\frac{dD'}{dt} = -D_s D' - B_s B' - A_s A' + \eta_s \eta', \tag{11}$$

$$\frac{dA'}{dt} = -A_s D' + fB' - D_s A', \tag{12}$$

$$\frac{dB'}{dt} = -B_s D' - D_s B' - fA', \tag{13}$$

$$\frac{d\eta'}{dt} = -\eta_s D' - D_s \eta'. \tag{14}$$

For exponential solutions of the form $e^{\lambda t}$ the eigenvalues λ satisfy the relationship

$$(\lambda + D_s)^2 = -0.5\{\eta_s^2 + f^2 - A_s^2 - B_s^2 \pm [(\eta_s^2 + f^2 - A_s^2 - B_s^2)^2 - 4f^2\eta_s^2]^{\frac{1}{2}}\}. \tag{15}$$

The real part of λ indicates how the solutions decay or grow exponentially with time. The maximum value for the real part of the nondimensional eigenvalue $\lambda^* = \mathrm{Re}(\lambda/f)$, from the four possible values given by (15), is depicted in Fig. 1 for several values of the nondimensional parameters $\mu^* = \mu/f$, $\nabla^2\phi^* = \nabla^2\phi/f^2$, $c_g^* = (1/f)(A_g^2 + B_g^2)^{\frac{1}{2}}$.

Regions where λ^* is less than zero indicate that the solution is stable. Unbalanced initial states would tend to the steady solutions on time scales of $-\lambda^{-1}$ for the stable cases.

For circular pressure patterns ($C_g^* = 0$) all the solutions are stable. Viscosity stabilizes the solutions, while increasing values of C_g^* have the opposite effect. Fig. 1 shows also that in the stable regions, the larger the negative values of $\nabla^2\phi^*$ are in magnitude the larger $|\lambda^*|$ becomes. Thus, flow patterns with strongly negative $\nabla^2\phi^*$ (strong high-pressure centers) tend to the steady state faster than weaker pressure configurations.

Fig. 2 depicts the steady-state nondimensional divergence $D^* = (D_s - \mu)/f$. The thick dashed line shows the axis of maximum divergence while the thick solid line represents the axis of maximum convergence. With these axis four regions can be easily delineated. In regions I and II increasing values of the drag coefficient lead first to an increase and then a decrease of divergence and in regions III and IV similar behavior is observed for convergence. These results are analogous to those obtained by Mahrt (1975) when reduced to the case of constant geostrophic vorticity. The present solutions do not contain the restriction of small Rossby number (Ro), and suggest that this behavior is valid over a large range of Ro. Regions I and III are similar to classical Ekman flow.

Not all of the Regions shown in Fig. 2 are equally likely to be realized as C_g^* changes, since for large C_g^* region III has unstable flow. As C_g^* is increased, the dividing line between regions III and IV tends toward the line which separates stable from unstable flow.

Fig. 3 depicts the nondimensional absolute vorticity

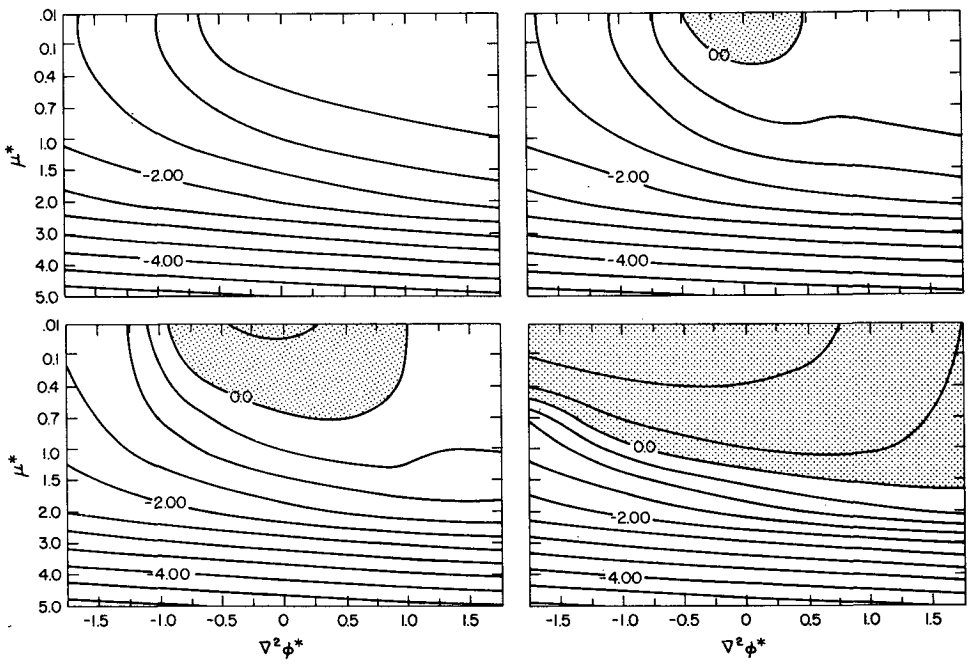

FIG. 1. Maximum value of the nondimensional eigenvalue λ^* for $C_g = 0$ (upper left), $C_g^* = 0.5$ (upper right), $C_g^* = 1$ (lower left) and $C_g^* = 2$ (lower right). Shaded areas indicate unstable regions. Analysis interval is 0.5.

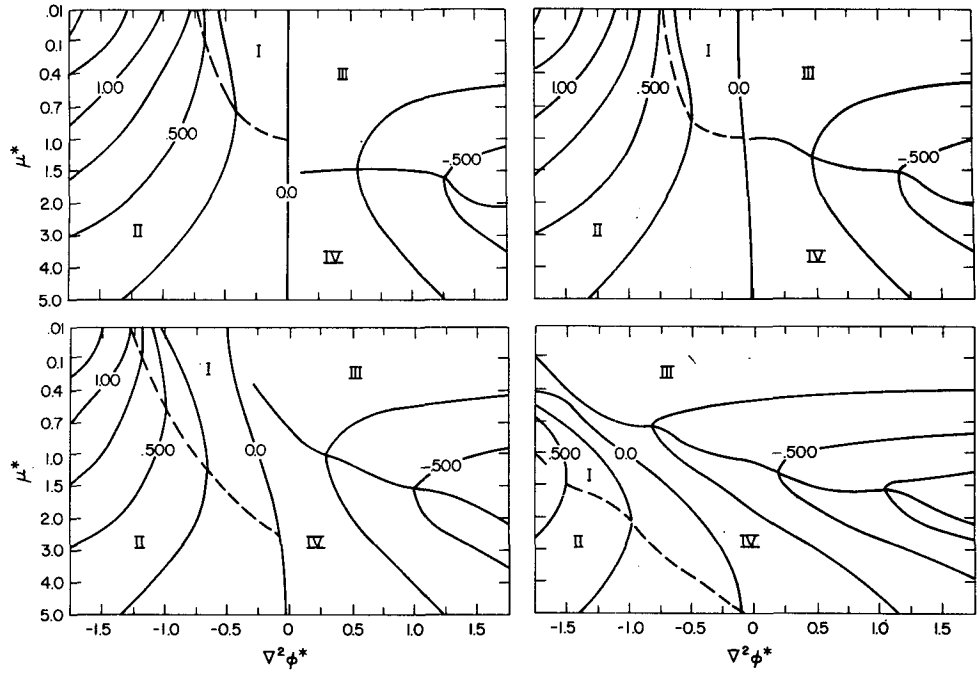

FIG. 2. As in Fig. 1 for nondimensional divergence D^*, in intervals of 0.25. Thick dashed lines indicate axis of divergence, and thick solid lines indicate axis of convergence. See text for description of symbols I, II, III and IV.

$\eta^*=\eta_s/f$. The isopleth $\eta^*=1$ is, in general, also the dividing line between divergent and convergent flow, indicating that divergence is associated with anticyclonic relative vorticity and convergence with cyclonic relative vorticity. There are a few exceptional cases of purely divergent or rotational flow.

Region I is characterized by divergence in anticyclonic areas, and increasing viscosity has the effect of increasing divergence and decreasing anticyclonic relative vorticity. This is the region for which Holton and Colton's (1972) conclusions are valid. However, in the region where $2\nabla^2\phi+f^2+A_g^2+B_g^2<0$ the strongly

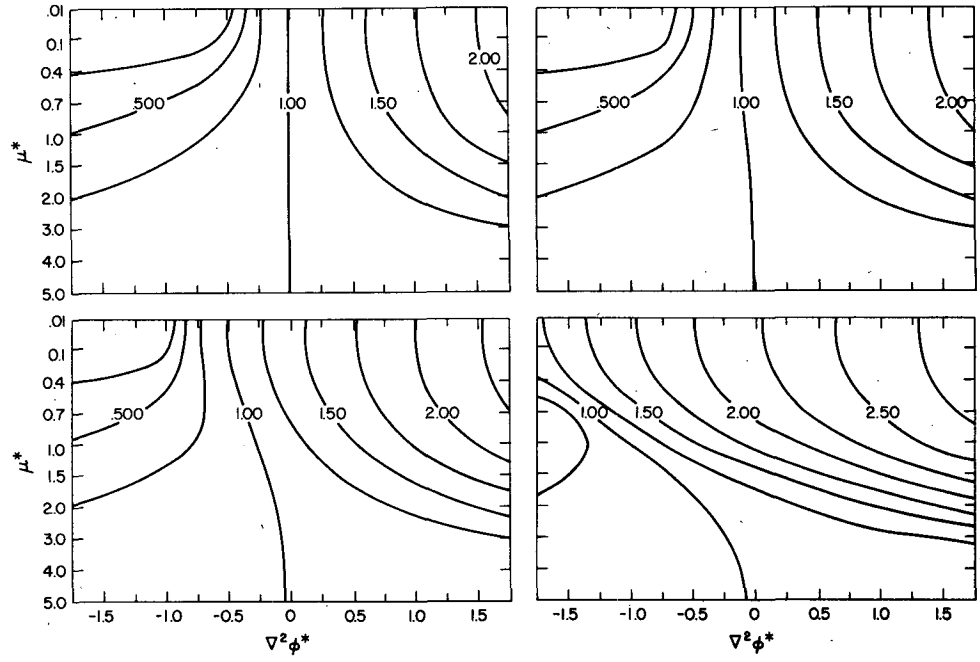

FIG. 3. As in Fig. 1 except for nondimensional vorticity η^* in intervals of 0.25.

divergent pressure gradient force seems to be a more likely basis for the generation of divergent flows than viscosity, since the divergence decreases with viscosity in region II. This conclusion is important since this type of flow tends to produce kinetic energy while viscosity tends to damp it.

This point is also made in Fig. 4. When $\nabla^2\phi^*$ becomes strongly negative, the divergence increases markedly; stronger viscosity tends to smooth out the divergence profile and damp D^*.

The nondimensional deformation

$$C_s^*=(1/f)(A_s^2+B_s^2)^{\frac{1}{2}}$$

is shown in Fig. 5. $C_s^*=0$ for $C_g^*=0$ and this case is not shown in this figure. Unstable flows are characterized by kinematic deformations which tend to the value of the geostrophic deformation for vanishingly small μ. Stable flows with strong friction, on the other hand, are all characterized by small deformations compared to the values of the geostrophic deformation. Thus well-mixed stable flows will tend to have more circular streamlines even if the pressure pattern has an elliptic geometry.

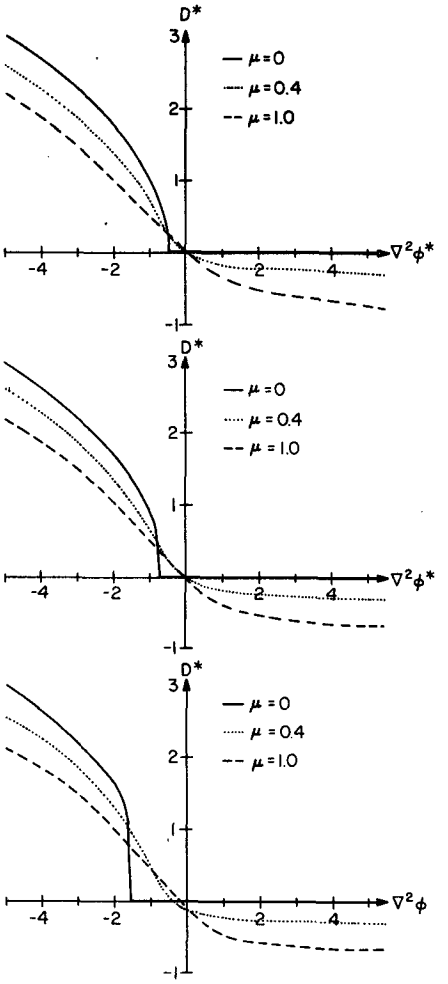

FIG. 4. Nondimensional divergence D^* as a function of $\nabla^2\phi^*$ for $C_g^*=0$, $C_g^*=0.4$ and $C_g^*=1$ from top to bottom of figure.

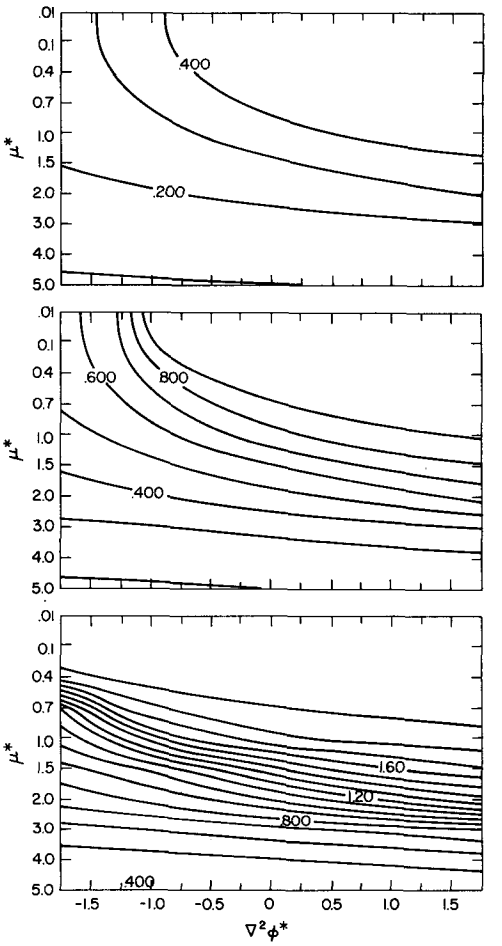

FIG. 5. Nondimensional deformation C^* for $C_g^*=0.5$, $C_g^*=1$ and $C_g^*=2$ from top to bottom of figure, in intervals of 0.1.

Circular or almost circular pressure patterns are of special interest, since many atmospheric systems have this geometry. Also for this case the solutions always appear to be stable. Thus, in the following section we will consider the particular case of $C_g^*=0$.

3. Circular pressure flows

In this case ($A_g=B_g=0$) the system of equations (1)–(4) becomes

$$\frac{dD}{dt}=\tfrac{1}{2}[\eta^2-(D^2+C^2)]-g, \tag{15}$$

$$\frac{dC}{dt}=-DC, \tag{16}$$

$$\frac{d\eta}{dt}=-\eta D+\mu f, \tag{17}$$

where

$$g=\nabla^2\phi+\tfrac{1}{2}(f^2-\mu^2),$$
$$C^2=A^2+B^2.$$

The Lagrangian steady-state solution for this case (Figs. 1–5) and Eq. (16) shows that $C_s=0$.

A linearized analysis in the neighborhood of the steady-state solution indicates that the integral curves in this region of the (D,η,C) phase space are given by

$$\rho=\rho_0\exp[(D_s/\eta_s)(\omega-\omega_0]=\frac{\rho_0}{C_0}C, \tag{18}$$

where the subscript 0 refers to the initial state, and ρ and ω are defined through the relationships

$$\left.\begin{aligned} D-D_s&=\rho\cos\omega\\ \eta-\eta_s&=\rho\sin\omega\end{aligned}\right\}. \tag{19}$$

These integral curves are three-dimensional spirals converging toward the point $(D_s,\eta_s,0)$. An infinite number of such spirals exists, each of them uniquely determined by the initial conditions.

Since $C_s=0$ for all values of μ for circular pressure fields, it may be of interest to consider the system of equations for the case for which $C=0$ initially, $C_g=0$, and thus $C=0$ always. For this case the system of equations reduces to Eqs. (15) and (17) with $C=0$. An analytic solution to this nonlinear system in D and η can be obtained.

This is done introducing the complex variable $W=\eta-iD$ and the complex constant $Z=\mu f+gi$. Then (15) and (17) are combined into a single nonlinear ordinary complex differential equation

$$\frac{dW}{dt}+\frac{i}{2}W^2=Z. \tag{20}$$

This is Riccatti's equation in the complex plane which can be easily solved if a particular solution W_p is known.

We take

$$W_p=re^{i\psi}, \tag{21}$$

where

$$r=\sqrt{2}(\mu^2f^2+g^2)^{\frac{1}{4}} \quad\text{and}\quad \psi=(3\pi/4)+\tfrac{1}{2}\tan^{-1}(g/\mu f).$$

Then

$$W=W_p\left[1+\frac{2}{[(W_p+W_0)(W_0-W_p)^{-1}]\exp(iW_pt)-1}\right],$$

or

$$\eta=\frac{\beta(r_s^2e^{-2\alpha t}-1)+2\alpha r_s\sin(\beta t+\psi_s)e^{-\alpha t}}{r_s^2e^{-2\alpha t}-2r_se^{-\alpha t}\cos(\beta t+\psi_s)+1},$$

$$D=\frac{-\alpha(r_s^2e^{-2\alpha t}-1)+2\beta r_s\sin(\beta t+\psi_s)e^{-\alpha t}}{r_s^2e^{-\alpha t}-2r_se^{-\alpha t}\cos(\beta t+\psi_s)+1},$$

where

$$\alpha=\mathrm{Im}(W_p),$$
$$\beta=\mathrm{Re}(W_p),$$
$$r_s^2=\frac{[(\rho_0/r)^2-1]+4(\rho_0/r)^2\sin^2(\theta_0+\psi)}{[1+(\rho_0^2/r^2)-2(\rho_0/r)\cos(\theta_0+\psi)]^2},$$
$$\psi_s=\tan^{-1}\left[\frac{2(\rho_0/r)\sin(\theta_0+\psi)}{(\rho_0^2/r^2)-1}\right],$$
$$\rho_0^2=\eta_0^2+D_0^2,$$
$$\theta_0=\tan^{-1}\left(\frac{D_0}{\eta_0}\right).$$

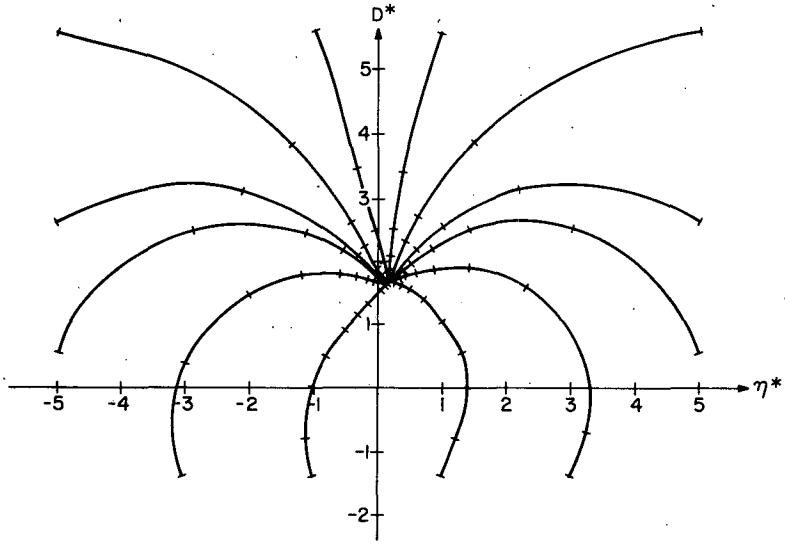

FIG. 6. Integral curves in (D^*,η^*) space from analytic solutions for the case $C=0$, $\mu^*=0.4$ and $\nabla^2\phi^*=-2.5$. Tic marks on curves are at intervals of $tf=0.25$.

Fig. 6 shows the integral curves in the (D^*,η^*) plane for a variety of initial conditions. It is easily recognized that these curves are spirals in the neighborhood of the stable singularity (D_s^*,η_s^*). The convergence rate of the finite-amplitude displacements from the steady-state is about as rapid in the present frictional case as in the frictionless analyses of I.

4. Conclusions

The present study emphasizes the sharp increase in flow divergence that accompanies a transition of the pressure field from a gradient to a supergradient condition. This may be the reason that several of MacDonald's supergradient (vergic) case studies show flow divergence strong enough (on the order of $f/2$) to be clearly obvious in objective synoptic scale data analysis.

Frictional damping in a time scale of 10^{-5} s^{-1} suggested by Holton and Colton (1974) produces a rather minor weakening of the supergradient divergence for any latitude more than about 10° away from the equator. However, as the ratio of μ/f exceeds 1, friction assumes an increasingly important role in the flow kinematics. Such large nondimensional values of friction may occur around the equator. Therefore, friction may be important to the flow kinematics of GATE data, as it appears to be to the energetics (Norquist *et al.*, 1977). However, in our preliminary analysis of some strongly disturbed phase III cases, it appears that even here, the generating mechanism of upper tropospheric flow divergence is the supergradient phenomena rather than friction (which may substantially weaken the divergence).

The source of the upper level supergradient pressure fields is likely to be the strong latent heating of pronounced convection, acting in conjunction with lower tropospheric mass convergence. The problem of transient mass-flow adjustment in a nonadiabatic, essentially baroclinic situation has not been considered. Our continuing investigation addresses this problem in an idealized approach. The results suggest that the rate of heating that may be required to maintain a supergradient pressure field outside the immediate equatorial regime is associated with precipitation rates in excess of 3 cm day^{-1}. Such strong precipitation is likely to be organized in narrow convective bands and may be difficult to measure with any standard raingage network, especially over the oceans. In view of this, the main utility of the presently proposed diagnosis of the phenomena through the upper tropospheric pressure fields may lie in the fact that, outside the deep tropics, these pressure fields are relatively easier to resolve with a standard synoptic-scale radiosonde observing network.

Acknowledgments. We would like to thank Dr. G. Árnason for helpful discussions. Partial support for this research was provided by the National Science Foundation under Grant ATM-77-17349.

REFERENCES

Holton, J. R., and D. E. Colton, 1972: A diagnostic study of the vorticity balance at 200 mb in the tropics during the northern summer. *J. Atmos. Sci.*, **30**, 1287–1302.

Lindzen, R. S., 1974: Wave-CISK in the tropics. *J. Atmos. Sci.*, **31**, 156–179.

MacDonald, A. E., 1977: On a type of strongly divergent steady state. *Mon. Wea. Rev.*, **105**, 771–785.

Mahrt, L., 1975: The influence of momentum advections on a well-mixed layer. *Quart. J. Roy. Meteor. Soc.*, **101**, 1–11.

Miyakoda, K., 1956: On a method of solving the balance equation. *J. Meteor. Soc. Japan*, **34**, 364–367.

Norquist, D. C., E. E. Recker and R. J. Reed, 1977: The energetics of African wave disturbances as observed during Phase III of GATE. *Mon. Wea. Rev.*, **105**, 334–342.

Paegle, J., and J. N. Paegle, 1974: An efficient and accurate approximation to the balance wind with application to non-elliptic data. *Mon. Wea. Rev.*, **102**, 838–846.

——, and ——, 1976a: On geopotential data and ellipticity of the balance equation: A data study. *Mon. Wea. Rev.*, **104**, 1279–1288.

Paegle, J. N., and J. Paegle, 1976b: On the realizability of strongly divergent supergradient flows. *J. Atmos. Sci.*, **33**, 2300–2307.

Reed, R. J., and R. H. Johnson, 1974: The vorticity budget of synoptic-scale wave disturbances in the tropical western Pacific. *J. Atmos. Sci.*, **31**, 1784–1790.

Syono, S., 1948: On the mechanism of the outburst of cold air from the polar cap. *J. Meteor. Soc. Japan*, **26**, 1–14.